PHYSICS AND CHEMISTRY OF SOLID STATE
V. 26, No. 1 (2025) pp. 10-22
Section: Physics

DOI: 10.15330/pcss.26.1.10-22

Vasyl Stefanyk Precarpathian National University

ФІЗИКА І ХІМІЯ ТВЕРДОГО ТІЛА
Т. 26, № 1 (2025) С. 10-22
Фізико-математичні науки

PACS: 84.60.Jt; 71.15.Mb

ISSN 1729-4428 (Print)
ISSN 2309-8589 (Online)

A. Meena[1], J.K. Bairwa[1], S. Kumari[1], U. Rani[2], P.K. Kamlesh[4], A.P. Singh[1], A.S. Verma[3,5]

Structural, electronic and optoelectronic characteristics by first principles calculations for $CH_3NH_3PbBr_3$ hybrid perovskite

[1]Department of Physics, University of Rajasthan, Jaipur, Rajasthan, India;
[2]Department of Physics, Noida Institute of Engineering and Technology, Greater Noida, India;
[3]Division of Research & Innovation, School of Applied and Life Sciences, Uttaranchal University, Dehradun, Uttarakhand, India;
[4]School of Basic and Applied Sciences, Nirwan University Jaipur, Jaipur, Rajasthan, India;
[5]University Centre for Research & Development, Department of Physics, Chandigarh University, Mohali, Punjab, India,
ajay_phy@rediffmail.com

Employing the Wien2k code, first-principles calculations within the full potential linearized augmented plane wave (FP-LAPW) method and density functional theory (DFT) framework were utilized to determine lattice constants, interatomic distances, density of states, and band structures. Three different exchange-correlation potentials, PBE, Local Density Approximation ("LDA"), and Wo-Cohen Generalized Gradient Approximation ("WC-GGA"), were employed for evaluating structural and electronic properties. The computed lattice constants and bulk modulus were found to be in excellent agreement with experimental data, validating the accuracy of the computational approach. The Goldsmith tolerance factor and octahedral factor were computed to confirm the structural stability of the material. The direct energy band gap of 2.32 eV observed at the R-R point suggests favourable conditions for solar applications. Further improvement in the band gap was achieved using the mBJ method. The optical properties, including the dielectric function, index of refraction, extinction coefficient, absorption coefficient, reflectivity, electron energy loss function, and photoconductivity, were systematically analysed. Notably, the study reveals the reliability of $CH_3NH_3PbBr_3$ as an absorption layer in solar cells, supported by the enhanced band gap and other optical properties.

Keywords: WIEN2k, DFT, Metal lead halide perovskites (MLHP), Solar cell, Optoelectronics.

Received 29 March 2024; Accepted 29 January 2025.

Introduction

In recent few years, the applications of generally structured ABX_3 metal lead halide perovskites (MLHP) have proven their uniqueness [1-2]. Perovskite compounds are rapidly used in optoelectronic devices and radiation detectors in terms of their applications [3-5]. The MLHP solar mechanization has emerged as admissible candidate that ensures the optoelectronic properties with higher accuracy [6-13]. Photovoltaic applications have produced remarkable growth [14-16]. Current research is being focused on the mixed cation, mixed halide, or mostly iodide-rich mixed halide perovskites [17,18] because iodine-based perovskites have much more suitable bandgap for ideal photovoltaic devices than bromine-based perovskites having wider bandgap (E_g > 2 eV) [19]. Mixed halides (I, Br, Cl) have shown a strong impact on the device's performance and stability. A small addition of Br and Cl confers the increased stability to the device as compared to pure iodine ($CH_3NH_3PbI_3$) based devices. Addition of Cl to $CH_3NH_3PbBr_3$ films improves the open circuit voltage and recombination rate constant. $MAPbBr_3$ has a shorter lattice constant, higher bandgap, higher cohesion energy and lower phase transition temperature as compared to $MAPbI_3$. [20-23]. Indeed, the highly efficient perovskite

solar cells use the more thermally stable $HC(NH_2)_2PbI_3$ with inclusions of small amounts of Cs^+, Br^-, and $CH_3NH_3^+$ to provide better structural stability, and further increasing for thermal stability of the material [24]. Metal lead halide perovskites have proved their superiority over the conventional solar cell because they have low cost and can be fabricated easily. The attractive room temperature processing and remarkable constitution with earth elements make them superior for photovoltaic applications [25-26]. These materials exhibit unique electronic and magnetic properties such as high carrier diffusion length, low surface combination velocity as well as high electron mobility [27-30]. Furthermore, these MLHP solar cells may have another distinct advantages such as the band gap of $MA(CH_3NH_3)PbX_3$ can easily be tuned and the appropriate features can be used to create colorful solar designs [31-33]. $MAPb(I_{1-x}Br_x)_3$ perovskites, have been studied to find out the colorful solar cells with low production cost, high-efficiency, and long-term stability [34]. Mostly, $MAPbBr_3$ perovskite shows the cubic phase (α) and space group (Pm3m) at greater temperature 236.9 K whereas tetragonal phase (β) and space group (I4/mcm) has been reflected at 155.1-236.9 K. Further orthorhombic phase (δ) and space group ($Pna2_1$) has been reflected at low temperatures [35]. This is a p-type semiconducting material with a direct band gap of 1.93-2.3 eV corresponding to an absorption onset of ⩽ 550 nm which makes this material an excellent light harvester [36-37]. In this regard density functional theory plays a key role in determining the electronic structures of $CH_3NH_3PbX_3$(X = Cl, Br, I) [38-39]. Also, the bandgap value of $MAPb(I_{1-x}Br_x)_3$, ($0 \leq x \leq 1$) material increasing as concentration of Br increases [40]. Jishi et al [41] have calculated the band structure of $CH_3NH_3PbBr_3$ using the mBJ potential that is found to be 2.23 eV. Feng et al [42] have successfully determined the band gap for tetragonal and orthorhombic $CH_3NH_3PbX_3$ (X = I and Br) crystal structure by the DFT+D2 method which are found to be in the range of 1.63 to 2.3 eV. Mosconi et al [43] have used accurate DFT and GW methods including spin-orbit coupling and calculated the expected band gap increasing moving from X=I to Cl.

Here, we aim to find out the different physical properties such as structural, optical and electronic properties of $CH_3NH_3PbBr_3$ perovskite materials by means of first-principles calculations in framework of DFT using Wien2k code. Estimation of optoelectronic properties will be helpful in the determination of electronic band structure of the perovskite as well as to ensure the capability of these materials using as absorbing substrate for solar cell structure. Stability of structure is measured in terms of octahedral and Goldsmith tolerance factor. Numerous studies of $CH_3NH_3PbX_3$ perovskites were reported recently but mostly focused on MLHP using I and Cl as halides whether they are single or as a mixture of halides. Only a few papers specifically reported the optical constants of $CH_3NH_3PbBr_3$ perovskite. In this study, we have investigated comprehensive optical constants and dielectric function for $CH_3NH_3PbBr_3$ perovskite which is in good agreement with researchers work as they obtained approximately 3.8-5.1 for the dielectric and the observed value is found smaller as compared to $CH_3NH_3PbI_3$ perovskite [44, 45, 19].

I. Formability of $CH_3NH_3PbBr_3$ Perovskite Structure:

ABX_3 structured metal lead halide perovskites have been proved as a family of efficient perovskites for optoelectronic applications. This is shown by figure 1 where A corresponds to organic cation of large size ($CH_3NH_3^+$), B is related to metallic cation Pb^{2+}, and Br represents halide ions making bonds to both the cations [46]. It has been studied that the perovskite structure is not completely cubic but is in a slightly deformed state. The properties such as ferromagnetism, superconductivity, ferroelectricity etc. are exhibited due to deformation of the perovskite structure. These properties of the material can be adjusted for photovoltaic applications. For the purpose, here we require to evolve some computational techniques with the help of which the electronic structure of material can be determined accurately. First-principles calculations have proved to be a milestone in determining important physical and chemical properties with high degree of accuracy.

The formability of stability of $CH_3NH_3PbBr_3$ perovskite structure has been systematically investigated using the tolerance factor–octahedral factor map method. The Goldschmidt tolerance factor (t) [47], which is given

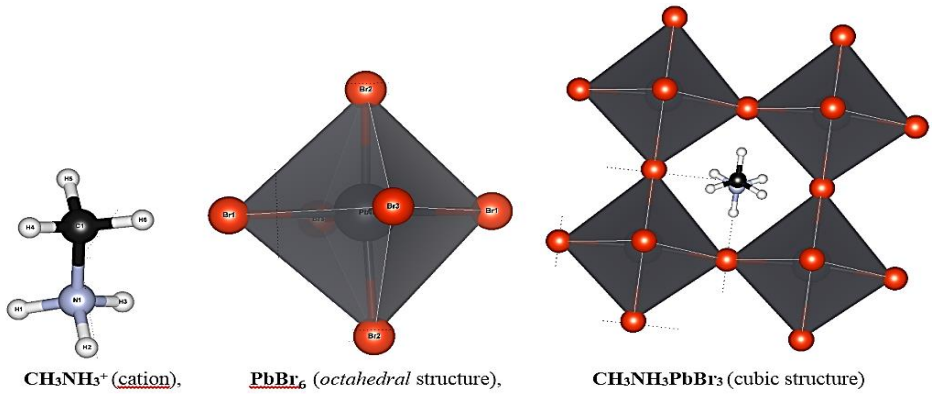

Fig. 1. Polyhedral representation of $CH_3NH_3PbBr_3$; Pb atoms are represented by the dark bluish grey spheres inside the octahedral; the Br atoms are dark red spheres at the octahedral corners; $PbBr_6$ is shown as black octahedral.

as: $t = (r_A + r_x)/\sqrt{2(r_B + r_x)}$

Here r_A, r_B and r_x are radii of organic group, metallic ion, and halogen ion respectively. An ideal cubic perovskite is expected when t = 1. The too large value of cation A in the ABX_3 structure makes t > 1, while a too small value of cation A makes t < 0.8. This position is indicative of the no perovskite nature of the structure [48, 49]. Mostly for stable perovskite structures, values are determined by $0.813 \leq t \leq 1.107$ [50]. This particular criterion is still applicable for MLHP what was formulated for organic perovskite structures. Stability is also determined in terms of other constant, such constant are called octahedral factor and are denoted by μ. This factor is determined by the ratio of r_B and r_x [51]. The value of μ smaller than 0.414, leads to unstable octahedral structure whereas slightly greater than 0.414, representing the contact of B cation with six X anions lead to a stabilize BX_6 octahedral structure. The following criterion confirms the stability for the structures, $0.414 \leq \mu < 0.592$ [52-54]. In Table 1, the $CH_3NH_3PbBr_3$ perovskite was calculated for tolerance factors t and octahedral factor μ based on effective ionic radii (in Å). In case, the larger cation $(CH_3NH_3)^+$ the effective radii r_A (A = CH_3NH_3) considered as an organic. Thus, we may estimate t as one half the C-N bond length (1.497 Å) plus the ionic radius of nitrogen (1.46 Å) [55]. The effective radii found between 1.60 and 2.50 considered as the perovskite [56].

II. Computational Methodology:

The calculations conducted in this study represent a first-principles investigative approach, known for its systematic and dependable methodology in elucidating the structural, electronic, and optical properties of materials. Ideally FP- LAPW method has been chosen for calculations [57-59] which is executed in WIEN2k code [60]. Kohn-Sham equation is solved under the density functional theory model. Through this procedure the ground state density and total energy of the system can be extracted in effective manner [61-63]. Further local density approximation (LDA) [64] and generalized gradient approximation (GGA) by Perdew, Burke and Ernzerhof (PBE) [65], popular methods have been used to deal with the Kohn-Sham (KS) equations. LDA is not able to deal with the electronic and magnetic properties corresponds to strongly correlated system. GGA adds all the approximations containing semi core corrections that arrange precise results throughout DFT simulations. However, LDA approximations are preferred over GGA approximations from a computational point of view because of its simplicity [66]. An exchange potential was recently proposed by Becke and Johnson (BJ), designed to yield the exact exchange potential in atoms [67-68]. Tran and Blaha was proposed a simple modification of the BJ potential [69-70]. In this method, known as TB-mBJ, the exchange potential is given by:

$$V_x^{TB-mBJ}(r) = cV_x^{BR}(r) + (3c-2)1/\pi(5/12)^{1/2}[2t(r)/\rho(r)]^{1/2} \quad (1)$$

Here ρ(r) is the electron density, t(r) the Kohn−Sham (KS) kinetic energy density, and $V_x^{BR}(r)$ the Becke−Roussel exchange potential [60]. In the TB-mBJ potential given in equation (1)

$$c = A + B(g)^{1/2} \quad (2)$$

$$g = \frac{1}{\Omega}\int \frac{1}{2}\left(\frac{|\nabla\rho_\uparrow(r)|}{\rho_\uparrow(r)} + \frac{|\nabla\rho_\downarrow(r)|}{\rho_\downarrow(r)}\right) d^3r$$

Here, the average of $|\nabla\rho/\rho|$ over the unit cell of volume Ω.

However, in this case Koller, Tran, and Blaha to improve the band gap prediction, [71-72] consider a more general form for c

$$c = A + Bg^e \quad (3)$$

Here the parameters A, B, and e values are 0.267, 0.656 and 1 respectively, were chosen because they produce the fit to the experimental band gaps of many semiconductors. Radi and other co-workers [41, 55] have calculated band structure using mBJ-method for several metal lead halide perovskite compounds that were found in good agreement with experimental values. Therefore, calculations for electronic structure of crystals with large unit cells, these methods may be easily used. However, the usefulness of this method is impeachment by its high computational cost.

In this work, all the structures studied taking the experimental unit cell data as input. The dependence on energy density of all physical properties makes it mathematically mandatory that minimizes the energy ensuring a stable structure. The energy minimization is measured as the energy

Table 1.

Structural equilibrium parameters; lattice constant, unit cell volume, Bulk modulus and derivative of bulk modulus for $CH_3NH_3PbBr_3$.

Properties	PBE	LDA	WC	Other calculation	
				Experimental	Theoretical
A (Å)	5.976	5.872	5.92	5.933 **[41],** 6.08 **[19]**	5.92 **[76]**, 5.94**[79]**, 5.90 **[35]**
V (Å)^3	213.482	202.52	207.53	225 **[19]**	206.3**[79]**, 208.8 **[31]**
B (GPa)	46.185	51.181	48.301	-	-
B' (GPa)	3.7604	4.0103	3.906	-	-

derivative of cell volume that has been fitted to the Murnaghan's equation of state [73, 74] provides equilibrium lattice constants, minimum energy value, the bulk modulus, its pressure derivative, and volume for the stable structure. To solve the KS equation, the space is considered as it is the integral form of two parts, one of which represent the Muffin Tin spheres and the other is considered as the interstitial region. The FP- LAPW method plays a key role in informing about KS orbital expansion. In the interstitial region, the KS orbital expansion understood as plane waves and assumed to be atomic like within the Muffin Tin spheres. The calculated radii (bohr) correspond to muffin-tin spheres are 2.5, 2.49, 1.16, 1.22 and 0.62 for Pb, Br, N, C and H atoms respectively. The angular momentum is understood $l_{max} = 10$ within the Muffin Tin spheres. As the Muffin Tin radius of hydrogen atom gets very close to R_H valued 0.62; the expansion of KS orbitals automatically settled for the required $R_H K_{max} = 3$ within the interstitial regions. Monkhorst-Pack scheme [75] with 5x5x5 grids is taken for the sampling of k-point within the Brillouin zone. The charge density is plane-wave expansion cut off G_{max}, where $G_{max} = 20$ bohr^{-1} for $CH_3NH_3PbBr_3$. The total energy (ec) tolerance of 0.1 mRy, a charge convergence (cc) of 0.0001e and internal force of 0.1 mRy/a.u. are grasped to make convergence within the frame of self-consistent calculations.

III. Results and Discussion:

3.1. Structural Properties:

Fundamentally the physical structure is constructed of unit cell. Here simple cubic unit cell constructs the

ABX_3 cubic perovskite structure by periodicity where atom B are located at the corners which are octahedrally coordinated by six halogen atoms. Experimentally the phases of compound $CH_3NH_3PbBr_3$ varies as the variation in temperature takes place. On studying the given compound, it has been found that at lower temperature the compound exists in orthorhombic phase whereas at medium temperature the compound exhibits the tetragonal phase and similarly pseudo cubic phase has also been observed at high temperature [35].

For the sake of mathematical simplicity, the cubic phase has been taken into considerations and here the optical, structural, and electronic properties of $CH_3NH_3PbBr_3$ perovskite material have been discussed. First of all, optimization for internal atomic positions have been considered to ensure the structural properties and then the optimization of lattice constants with different potential (PBE, LDA, WC-GGA) is done by minimizing the total energy under the consideration of total energy as a function of volume as well as graphical fitting of Energy Volume (E-V) curve with Murnaghan's equation [74] (fig. 2), we get the data related to the structural properties $CH_3NH_3PbBr_3$ compound. The calculated structural properties data from various approximations are shown in Table 1 with their comparisons of available experimental as well as theoretical results. Experimentally described lattice constant for $CH_3NH_3PbBr_3$ is, a=5.92 Å [76], a=5.94Å [77] and the calculation by WC-GGA approximations confirm the value 5.92 Å. The calculated lattice constants and volume values of the present work are in good agreement with the theoretical values because of practicing different method of calculation. Moreover, the matching of the calculated values with the experimental values, assures the reliability of the applied method.

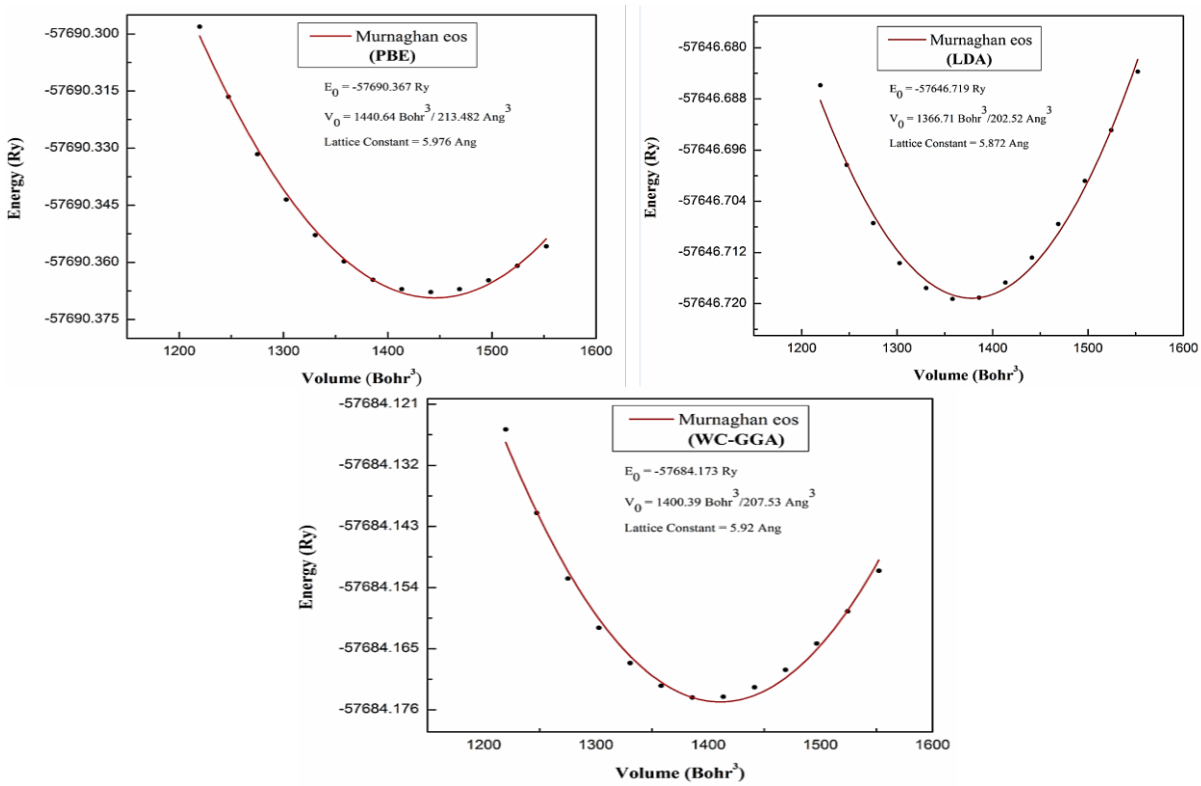

Fig. 2. Total energy versus volume curve with different exchange correlation potentials.

3.2. Electronic properties:

3.2.1. Band Structure Curves:

Band structure curves provide important information about the crystal structure. All the calculations that are related to band structure of the material have been shown in table 2 under the consideration of PBE and LDA approximations, we found the bang gap are shown in fig. 3. Here energy function plot has been considered for the first Brillouin zone. The difference in between valance band maximum (VBM) and conduction band minimum (CBM) calculates the band gap. The value of the bandgap is improved by using the mBJ method, it is just an exchange potential that can be used in combination with a LDA correlation potential and are improved further by using the KTB-mBJ method. However, the improvement in the bandgap is found slightly far above the experimental values using these parameter values in the KTB-mBJ method. Thus, to improve the bang gap prediction, we consider a new set of values for the parameters. A and B are taken the same, but the parameter e (e = 0.5) is taken different, then we get exact bandgap in certain case. Thus, according to the band structure curves, it is resulted that this compound, by LDA and KTB-mBJ + LDA approximations, has direct band gap with 1.83 eV and 2.32 eV respectively at the R-point. According to the experimental results the values for direct band gap are described as by 2.3 eV and 2.35 eV [34,78].

This indicates that the calculated results show good agreement with the experimental results. Further it has also been studied that the dispersive nature of the conduction band is relatively higher than the valence band because of its delocalization when electronic transition takes place to some other higher energy states.

3.2.2. Density of States (DOS)

We have studied total density of states (TDOS) and partial density of states (PDOS) ofPb, Br, N, C and $CH_3NH_3^+$ cation with LDA and KTB-*mBJ* as exchange correlation potential in energy range (-6 to 8) *eV* as shown in figure 4(a) and (b). By the fig. 4, it is obvious that there are three different regions for total density of states; (−6 eV to -4 eV) defines the lower valence band while (−4 eV to 0 eV) defines upper valence band as well as lower conduction band. We have discussed the results of KTB-mBJ as exchange correlation potential as shown in figure 4(b). The lower valence band is defined mainly by $\mathrm{MA}-p$ orbitals and little bit contributed by $\mathrm{Br}-5p$ and $\mathrm{MA}-s$ state. The weak hybridization of $Br-5p$ with $\mathrm{Pb}-5s$ and $\mathrm{Pb}-6p$ state defines the upper valence band. The last region, the lower conduction bands (LCB) are prepared by the hybridization of $Br-5p$ and $\mathrm{Pb}-6p$ orbital.

Table 2.

Calculated band gap in eV with PBE, LDA approximation and KTB-mBJ method and comparison with other theoretical and experimental data.

Compound	PBE	LDA	PBE+KTB-mBJ	Other calculation	
				Experimental	Theoretical
$CH_3NH_3PbBr_3$	1.93	1.83	2.32	1.93-2.3 **[76]**, 2.30**[34]**, 2.35**[80]**	2.233**[41]**, 2.56**[43]**, 2.34**[82]**

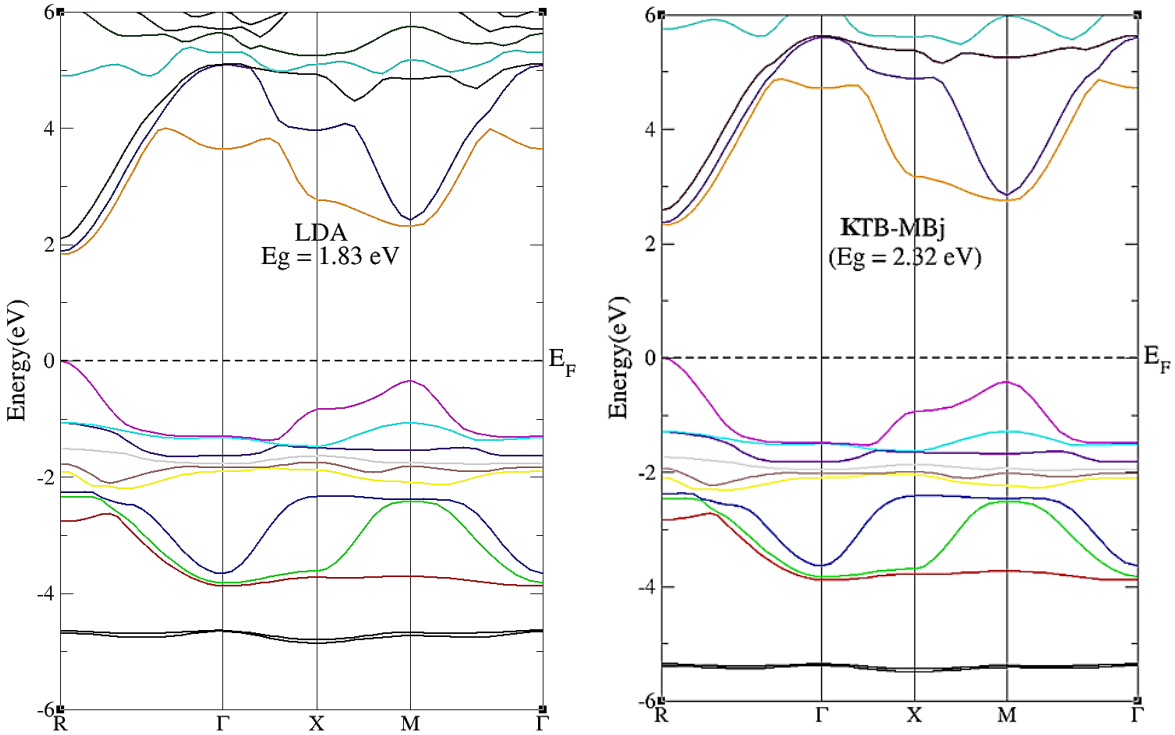

Fig. 3. Band structure of cubic phase of $CH_3NH_3PbBr_3$ perovskite with different exchange correlation potentials.

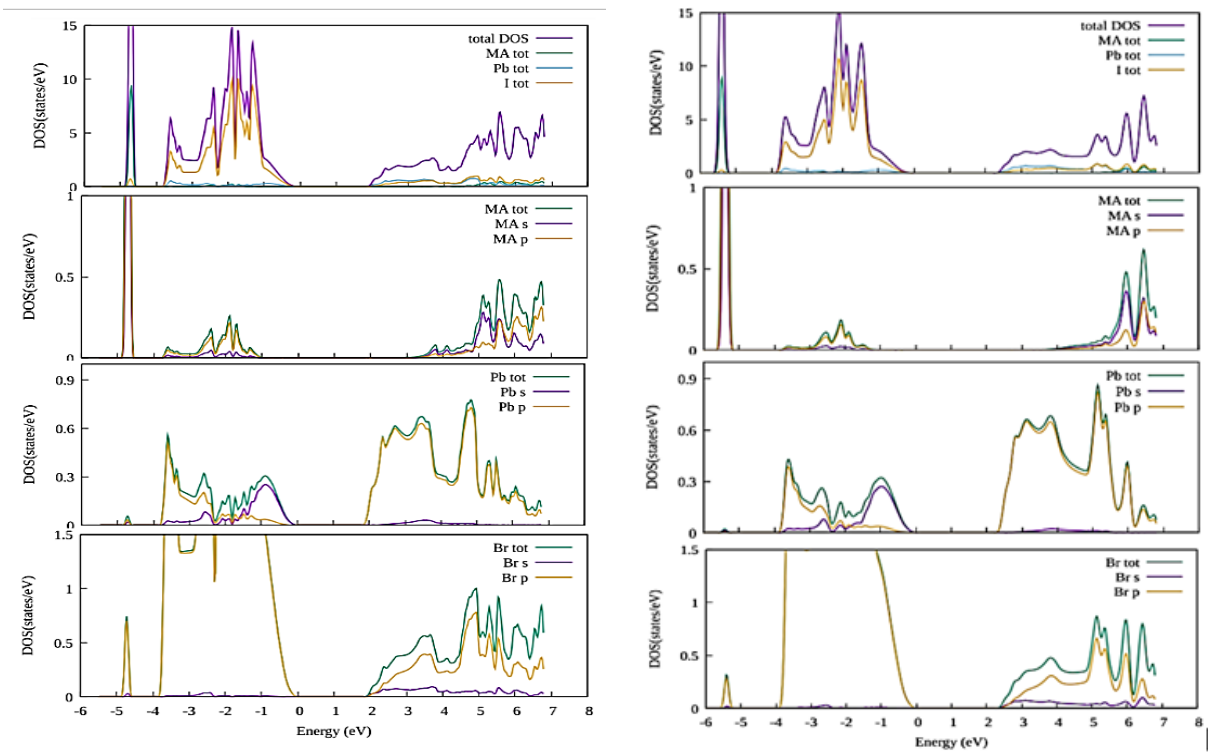

(a) (b)

Fig. 4. The density of states of $CH_3NH_3PbBr_3$ perovskite with exchange correlation potential (a) LDA and (b) KTB-mBJ.

3.3. Optical Properties:

Determining novel devices for generating renewable energy requires a thorough study about the optical properties of the material. Maxwell's relations macroscopically characterise the interaction of electromagnetic radiation with matter. These equations carry some specific constants used as parameters to find out the optical properties of the material. These characteristic constants are known as permittivity, permeability, and refractive indices of the medium. This has been theoretically proved that the above characteristics of the material are recognized to be dependent on frequency. Therefore, the dielectric function can be described as the complex variable of frequency given as $\varepsilon(\omega) = \varepsilon_1(\omega) + i\varepsilon_2(\omega)$. The momentum matrix calculates the imaginary part of the dielectric function $\varepsilon_2(\omega)$ and the elements of matrix represents the significance of wave functions corresponding to occupied and unoccupied levels. Mathematically the matrix is described by the following expression [19, 79,80].

$$\varepsilon_2(\omega) = \frac{2e^2\pi}{\Omega\varepsilon_0}\sum_{k,v,c}|\psi_k^c|u.r|\psi_k^v|^2\,\delta(E_k^c - E_k^v - E) \quad (4)$$

Here ω stands for phonon frequency, e stands for the charge of an electron and Ω stands for the volume of unit cell. ω have been considered as the unit vector along the polarization of the incident electric field, Ψ_{k^c} and Ψ_{k^v} are the descriptions for the wave function of conduction and valence band respectively corresponding to specific value of k. The Kramer-Kroning relations provides the real part$\varepsilon_1(\omega)$, which is evaluated from $\varepsilon_2(\omega)$ and is given by [19, 81]

$$\varepsilon_1(\omega) = 1 + \frac{2}{\pi}P\int_0^\infty \frac{\omega'\varepsilon_2(\omega')}{\omega'^2-\omega^2}d\omega' \quad (5)$$

All the optical properties and related information of the material like absorption coefficient (ω) , the index of refraction $n(\omega)$, the extinction coefficient, the optical conductivity $\sigma(\omega)$, the reflectivity $R(\omega)$, and the loss function can be deduced through dielectric function which is defined in terms of real and imaginary parts [82, 83]. The dielectric function is a complex physical quantity of which the real and imaginary parts have been shown according to figure 5 (a) and (b) respectively. The energy range of photon is considered up to 14 eV. The actual principal maxima correspond to the real part of dielectric function appears at energy of 3 eV. The main dominant transition in the spectra is due to the electronic transitions. These electronic transitions take places as electron makes transitions between upper valence band and bottom conduction band. Further there appears decreasing in the spectra up to 13.56 eV. The calculated roots for $\varepsilon_1(\omega)$ have been observed at energies of 5.15 eV and 10.76 eV. These observed root values of $\varepsilon_1(\omega)$ calculates what energy loss occurs there corresponding to the relevant energy. Totally there occurs high absorption corresponding to these energies (fig 6(a)). Apart this, the real part related dielectric function has shown the negative value in the energy range 10.78 eV- 13.56 eV. This has been caused for no possibility of wave propagation through the matter. The imaginary part $\varepsilon_2(\omega)$ also plays an important role in the determination of optical properties of material. Some significant changes in $\varepsilon_2(\omega)$ appears at energy 2.32 eV that are described by fig. 5(b). Optical transitions have been caused because of this energy. This is known as optical band gap. There appear two prominent peaks corresponding to 4 eV and 9 eV energies as an effect

of optical transitions. The first and principal peak of the curve arises there because of inter band transitions of electrons. The root cause for this phenomenon are the transitions that take places from occupied levels of valence band to unoccupied levels of conduction bands. Here the occupied levels of valence bands are Br-5p and Pb–6s while the unoccupied level of conduction band is Pb-6p. There are also some another transition of electrons taking places from the semi-core states to the conduction band causes the peaks at lower intensities. The static dielectric constant also has been calculated valued to be 4 ensuring the result is very close with other workers [19].

The $n(\omega)$ includes the real part as well as the imaginary part wherever the real part defines the refractive index, and the imaginary part defines the extinction coefficient that are plotted in figure 6. The refractive index behaves as a complex in nature, and it can significantly explain the propagation, dispersion as well as how the electromagnetic waves dissipate. The figure 6(a) signifies that initially the curve of refractive index attains the value of 2 at zero energy, such refractive index is said to be as static refractive index. It is also observed that refractive index increases because of increasing in energy of radiation. Thus, the refractive index attains its peak value

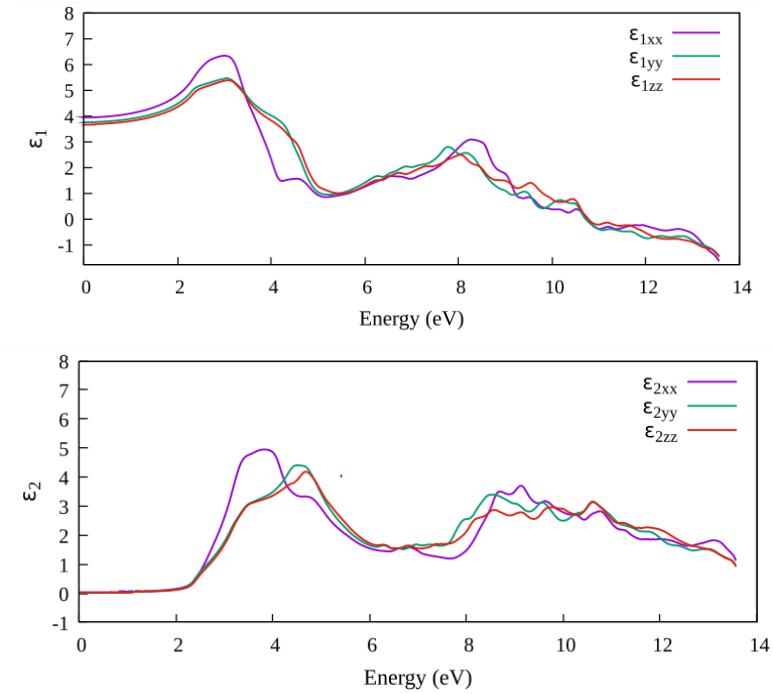

Fig. 5. The calculated real $\varepsilon_1(\omega)$ and imaginary $\varepsilon_2(\omega)$ parts of complex dielectric constant for $CH_3NH_3PbBr_3$.

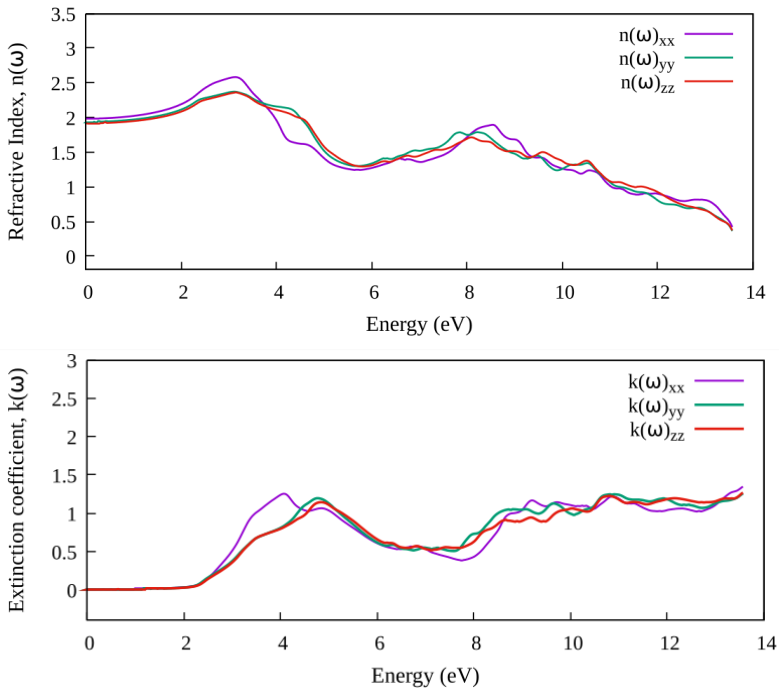

Fig. 6. (a) Refractive index n (w) and (b) Extinction coefficient versus photon energy for cubic perovskite $CH_3NH_3PbBr_3$.

2.58 at energy 3.14 eV. It is also clear from curve that the peak value of refractive index occurs only in the energy range of 2 eV to 4 eV that represents the visible range. The little difference in perpendicular direction of refractive indices valued by 0.04, confirms that material exhibits the isotropic behaviour as optical properties. The extinction coefficient versus light energy plot for $CH_3NH_3PbBr_3$ has been drawn Fig. 6(b). This is clear from the curve that the maxima of the curve appear at energy 4.06 eV wherever the extinction coefficient is observed to be 1.25.

This is the representation of large amount absorption at the given energy range that is confirmed by the absorption peak occurring in fig.7 (a). Also, the first minimum has been observed at energy 6.84 eV which indicates that the absorption corresponds to these energies is minimum. The same fact is also happening there in the absorption coefficient curve (fig.7 (a)). Moreover, the extinction coefficient mainly exists in the visible and ultraviolet region (3-6 eV); and the large mathematical value of absorption coefficient implies enough absorption of radiations but despite the radiation, the electrons are not able to retain enough energy that makes the inter band transitions.

As a result, Plasmon fluctuations take place within the crystal due to heat. The electron energy loss function plays the role of an optical parameter which is the measurement of what energy has been lost per unit length as fast electron passing through the material. The computed optical

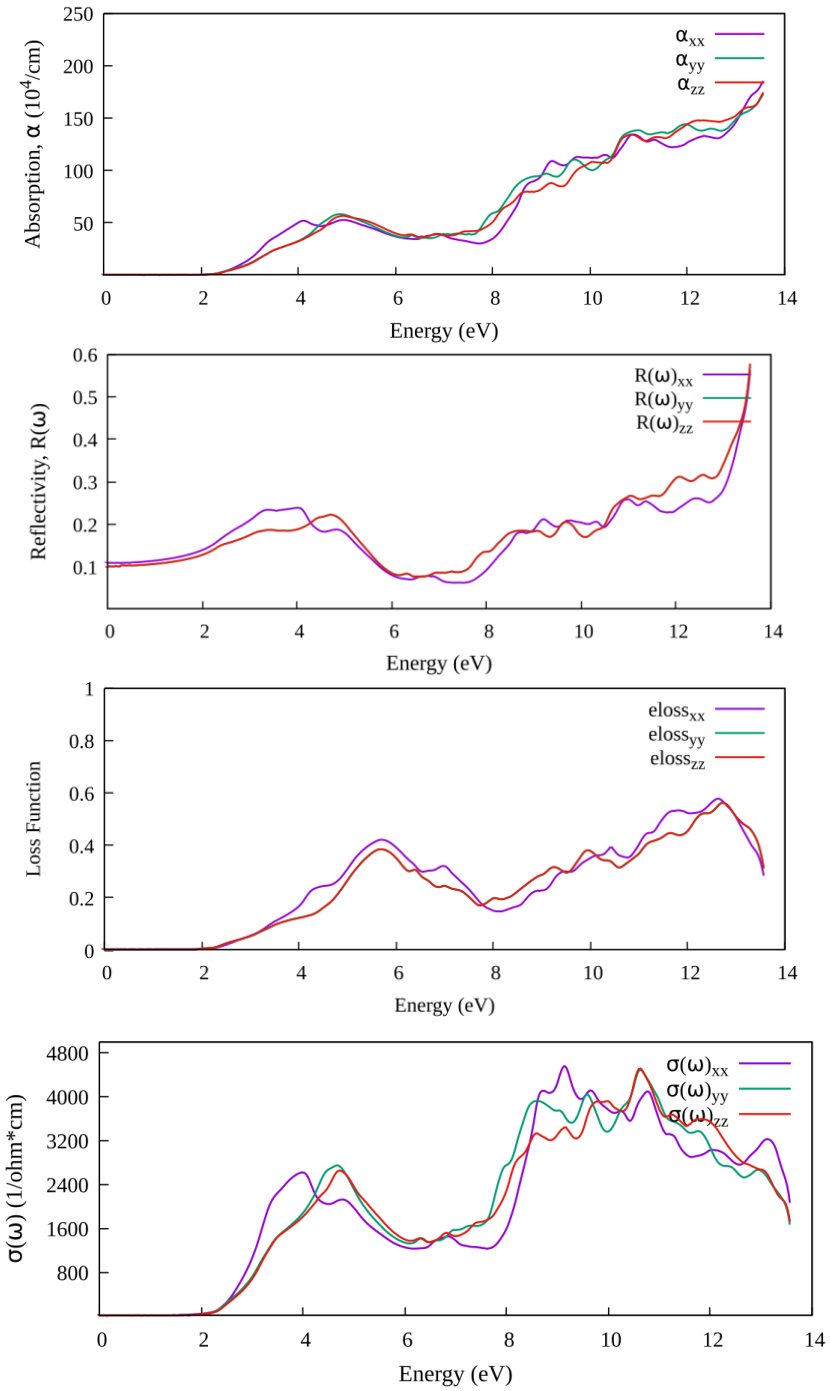

Fig.7. The calculated (a) absorption coefficient (b) reflectivity (c) electron energy loss function and (d) optical conductivity for $CH_3NH_3PbBr_3$ in cubic phase.

parameters of the investigated materials show their potential for efficient photovoltaic devices in near infra and visible regions whereas these may be good candidates for UV shields for higher energy spectrum. All these optical functions have been calculated with exchange correlation function KTB-mBJ is shown in fig.7 (a). The absorption edge takes place from optical band gap 2.32 eV that is related to direct R-R transition. Moreover, two minima exist there in the curve of $\varepsilon_1(\omega)$ having energy range of 4–10 eV (fig. 5(a)); the happening of two absorption peaks at this region (fig. 7(a)). This conclude that the compound reflects the significant absorption in the UV range and this process grows up within ultraviolet region as absorption peak with 5.25 eV and 9.40 eV occurring in UV region. This compound provides better absorption coefficient in the 9-14 eV region. Reflectivity measures how much light a substance reflects when exposed to it and is calculated by dividing the energy of the incident wave by the energy of the reflected wave. The reflectivity spectra of $CH_3NH_3PbBr_3$ as a function of photon energy are depicted in Fig. 7(b). In the infrared region, the value of optical reflectivity $R(\omega)$ increases as the energy of incident radiation rises; in the visible region it starts to decrease; further in the UV region, it increases with the energy of the electromagnetic radiation. Therefore, the highest reflectivity in these compounds is observed in the ultraviolet (UV) region; for the high UV region, it again starts to decrease. Hence the studied compounds can serve as excellent coating materials, particularly in the energy region spanning from 8 to 14 eV.

The energy loss function has been shown in Fig. 7 (c) that is the function of photon energy. The peak that occurs in the figure shows the maximum loss at the certain or specific energy. The highest loss appears because of collective behaviour of electrons that corresponds to Plasmon frequency. By comparison between the real roots of the dielectric function and peak of the loss function, the oscillating energy of the plasma of about 5.15 eV has been observed. Also, the leading peak has been appeared at 5.7 eV, which is the measurement of sharp reduction in energy for reflectivity [fig. 7(b)]. Thus, it has been concluded that wherever the real part ε_1 (ω) of the dielectric function disappears, this is caused for occurring abrupt drop in reflectivity within the curve resulting the leading peak in energy loss curve.

The measurement for the optical conductivities of $CH_3NH_3PbBr_3$ material is shown in fig 7(d). The optical conductivity is measured in terms of the photo-electric conversion efficiency, and it is used to measure the changes caused by the illumination. It is studied that the maximum value of photoconductivity for the material has been obtained at energy 9.5 eV corresponds to UV range and also peak at energy 3.9 eV corresponds to visible range that are the crucial conditions that makes $CH_3NH_3PbBr_3$ material to be potential candidate used as solar cell absorption layer.

Summary and Conclusion:

In this study, a comprehensive investigation into the structural, electronic, and optical properties of $CH_3NH_3PbBr_3$, a key material in Metal Lead Halide Perovskite (MLHP) solar cells, was conducted using first-principles calculations within the framework of density functional theory (DFT). The investigation revealed a direct energy band gap of 2.32 eV at the R-R point, positioning $CH_3NH_3PbBr_3$ as a promising material for solar applications. Optical properties demonstrate the material's suitability as an absorption layer in solar cells. The Goldsmith tolerance factor and octahedral factor were calculated, confirming the structural stability of $CH_3NH_3PbBr_3$.The research contributes valuable insights to the field of Metal Lead Halide Perovskites (MLHP) solar cells, highlighting the potential of $CH_3NH_3PbBr_3$ and providing a foundation for future developments. The calculated properties, in conjunction with the utilization of advanced computational methods, offer a deeper understanding of the material's behaviour, paving the way for further advancements in renewable energy technologies.

Meena A. – M.Sc. in Physics, Doctoral Student;
Bairwa J.K. – Ph.D. in Physics, Assistant Professor;
Kumari S. – Ph.D. in Physics, Associate Professor;
Rani U. – Ph.D. in Physics, Assistant Professor;
Kamlesh P.K. – Ph.D. in Physics, Associate Professor;
Singh A.P. – Ph.D. in Physics, Assistant Professor;
Verma A.S – Ph.D. in Physics, Professor, Corr. Author.

[1] A. Navrotsky, Energetics and Crystal Chemical Systematics among Ilmenite, Lithium Niobate, and Perovskite Structure, Chem. Mater., 10, 2787 (1998); http://dx.doi.org/10.1021/cm9801901.
[2] K. R. Kendall, C. Navas, J. K. Thomas, and H.-Conrad z. Loye, *Recent Developments in Oxide Ion Conductors: Aurivillius Phases*, Chem. Mater., 8, 642 (1996); https://doi.org/10.1021/cm9503083.
[3] J. M. D. Coey, M. Viret, and S. V. Molnar, *Mixed-valence manganites*, Adv Phys., 48(2), 167 (1999); https://doi.org/10.1080/000187399243455.
[4] B. Náfrádi, G. Náfrádi, L. Forró, and Endre Horváth, *Methylammonium Lead Iodide for Efficient X-ray Energy Conversion*. J. Phys. Chem. C, 119, 25204 (2015); https://doi.org/10.1021/acs.jpcc.5b07876.
[5] S. Yakunin, D. N. Dirin, Y. Shynkarenko, V. Morad, I. Cherniukh, O. Nazarenko, D. Kreil, T. Nauser, and M. V. Kovalenko, *Detection of gamma photons using solution-grown single crystals of hybrid lead halide perovskites*, Nat. Photonics, 10, 585 (2016).
[6] A. Kojima, K. Teshima, Y. Shirai, and T. Miyasaka, *Organometal Halide Perovskites as Visible-Light Sensitizers for Photovoltaic Cells*, J. Am. Chem. Soc., 131(17), 6050 (2009); https://doi.org/10.1021/ja809598r.
[7] H.-S. Kim, C.-R. Lee, J.-H. Im, K.-B. Lee, T. Moehl, A. Marchioro, S.-J. Moon, R. Humphry-Baker, J.-H. Yum, J. E. Moser, M. Gratzel, and N.-G. Park, *Lead Iodide Perovskite Sensitized All-Solid-State Submicron Thin Film Mesoscopic Solar Cell with Efficiency Exceeding 9%*, Sci. Rep., 2, 591 (2012); https://doi.org/10.1038/srep00591.

[8] U. Rani, P K Kamlesh, R. Singh, T. Kumar, R. Gupta, S. Al-Qaisi, K. Kaur, and A. S. Verma, *Exploring properties of organometallic double perovskite $(CH_3NH_3)_2AgInCl_6$: A novel material for energy conversion devices*, Mod Phys Lett B, 38(18), 2450144 (2023); https://doi.org/10.1142/S0217984924501446.

[9] U. Rani, P. K. Kamlesh, T. Kumar Joshi, S. Sharma, R. Gupta, T. Kumar, and A. S. Verma, *Computational investigation of inverse perovskite $SbPX_3$ (X = Mg, Ca, and Sr) structured materials with applicability in green energy resources*, Comput. Condens. Matter, 36, e00835 (2023); https://doi.org/10.1016/j.cocom.2023.e00835.

[10] M. Rani, P. K. Kamlesh, S. Kumawat, U. Rani, G. Arora, and A. S. Verma, *Rare earth-based oxides double perovskites A_2NiMnO_6 (A= La and gd): Applications in magneto-caloric, photo-catalytic and thermoelectric devices*, Physica B Condens. Matter, 415645 (2023); https://doi.org/10.1016/j.physb.2023.415645.

[11] Y. Soni, R. Agrawal, V. Yadav, P. Singh, S. Singh, U. Rani, and *A. S. Verma, Electronic and optical properties of novel double perovskite compound Cs_2RbInI_6*, J. Ovonic. Res., 19, 579 (2023); https://doi.org/10.15251/JOR.2023.195.579.

[12] U. Rani, P K Kamlesh, T. K. Joshi, R. Singh, S. Al-Qaisi, R. Gupta, T. Kumar, and A S Verma, *Electronic structure, theoretical power conversion efficiency, and thermoelectric properties of bismuth-based alkaline earth antiperovskites*, J Mol Model**,** 29, 329 (2023); https://doi.org/10.1007/s00894-023-05732-z.

[13] J. K. Bairwa, P K Kamlesh, U. Rani, R. Singh, R. Gupta, S. Kumari, T. Kumar, and A S Verma, *Highly efficient and stable Ra_2LaNbO_6 double perovskite for energy conversion device applications*, Mater Sci Energy Techno, 7, 61 (2024); https://doi.org/10.1016/j.mset.2023.07.005.

[14] P. Gao, M. Grätzel, and M. K. Nazeeruddin, *Organohalide lead perovskites for photovoltaic applications*, Energy Environ. Science, 7, 2448 (2014). https://doi.org/10.1039/C4EE00942H.

[15] K. C. Wang, J.Y. Jeng, P. S. Shen, Y. C. Chang, E. W- Guang Diau, C. H. Tsai, T. Y. Chao, H. C. Hsu, P. Y. Lin, P. Chen, T. F. Guo, and T. C. Wen, *p-type Mesoscopic Nickel Oxide/Organometallic Perovskite Heterojunction Solar Cells*, Sci. Reports, 4, 4756 (2014); https://doi.org/10.1038/srep04756.

[16] L. Huang, X. Cui, C. Liu, W. Yang, W. Shi, J. Lai, and L. Wang, *Improvement on performance of hybrid $CH_3NH_3PbI_{3-x}Cl_x$ perovskite solar cells induced sequential deposition by low pressure assisted solution processing*, Solar Energy, 199, 826 (2020); https://doi.org/10.1016/j.solener.2020.02.080.

[17] D.P. McMeekin, Z. Wang, W. Rehman, F. Pulvirenti, J. B. Patel, N. K. Noel, M. B. Johnston, S. R. Marder, L. M. Herz, and H. J. Snaith, *Crystallization Kinetics and Morphology Control of Formamidinium−Cesium Mixed-Cation Lead Mixed-Halide Perovskite via Tunability of the Colloidal Precursor Solution*, Adv. Mater., 29, 1607039 (2017); https://doi.org/10.1002/adma.201607039.

[18] D.P. Mcmeekin, G. Sadoughi, W. Rehman, G. E. Eperon, M. Saliba, M. T. Horantner, A. Haghighirad, N. Sakai, L. Korte, B. Rech, M. B. Johnston, L. M. Herz, And H. J. Snaith, *A Mixed-Cation Lead Mixed-Halide Perovskite Absorber for Tandem Solar Cells*. Science, 351, 151 (2016); https://doi.org/10.1126/science.aad5845.

[19] Md Roknuzzaman, K. Ostrikov, K. C. Wasalathilake, C. Yan, H. Wang, and T. Tesfamichael, *Insight into lead-free organic-inorganic hybrid perovskites for photovoltaics and optoelectronics: A first-principles study*, Org. Electron, 59, 99 (2018); https://doi.org/10.1016/j.orgel.2018.04.051.

[20] N. J. Jeon, J. H. Noh, Y. C. Kim, W. S. Yang, S. Ryu, and S. I. Seok, *Solvent engineering for high-performance inorganic-organic hybrid perovskite solar cells.* Nat. Mater., 13, 897 (2014); https://doi.org/10.1038/nmat4014.

[21] M. M. Lee, J. Teuscher, T. Miyasaka, T. N. Murakami, and H. J. Snaith, *Efficient hybrid solar cells based on meso-super structured organometal halide perovskites*. Science, 338, 643 (2012); https://doi.org/10.1126/science.1228604.

[22] E. Edri, S. Kirmayer, D. Cahen, and G. Hodes, *High open-circuit voltage solar cells based on organic-inorganic lead bromide perovskite*. J. Phys. Chem. Lett., 4, 897 (2013); https://doi.org/10.1021/jz400348q.

[23] M. Zhang, H. Yu, M. Lyu, Q. Wang, Q.; J.-H. Yun, L. Wang, *Composition-dependent photoluminescence intensity and prolonged recombination lifetime of perovskite $CH_3NH_3PbBr_{3-x}Cl_x$ films*. Chem. Commun., 50 11727 (2014); https://doi.org/10.1039/C4CC04973J.

[24] M. Saliba, T. Matsui, J. Y. Seo, K. Domanski, J. P. Correa-Baena, M. K. Nazeeruddin, S. M. Zakeeruddin, W. Tress, A. Abate, And A. Hagfeldt, *Cesium-Containing Triple Cation Perovskite Solar Cells: Improved Stability, Reproducibility and High Efficiency*, Energy Environ. Sci., 9, 1989 (2016); https://doi.org/10.1039/C5EE03874J.

[25] S. P. Singh, and P. Nagarjuna, *Organometal halide perovskites as useful materials in sensitized solar cells*, Dalton Trans., 43, 5247 (2014); https://doi.org/10.1039/C3DT53503G.

[26] S.A. Kulkarni, T. Baikie, P.P. Boix, N.Yantara, N. Mathews, and S. Mhaisalkar, *Band-gap tuning of lead halide perovskites using a sequential deposition process*, J. Mater. Chem. A, 2, 9221 (2014); https://doi.org/10.1039/C4TA00435C.

[27] I. Koutselas, P. Bampoulis, E. Maratou, T. Evagelinou, G. Pagona, and G. C. Papavassiliou, *Some Unconventional Organic−Inorganic Hybrid Low-Dimensional Semiconductors and Related Light-Emitting Devices*, J. Phys. Chem. C, 115, 8475 (2011); https://doi.org/10.1021/jp111881b.

[28] C. R. Li, H. T. Deng, J. Wan, Y. Y. Zheng, and W. J. Dong, *Photoconductive properties of organic–inorganic hybrid perovskite $(C_6H_{13}NH_3)_2(CH_3NH_3)_{m-1}Pb_mI_{3m+1}$:$TiO_2$ nanocomposites device structure*, Mater.Lett., 64, 2735 (2010); https://doi.org/10.1016/j.matlet.2010.09.018.

[29] G.S. Patrin, N.V. Volkov, and I.V. Prokhorova, *Nonlinear magnetic resonance in the $(CH_3NH_3)_2CuBr_4$ crystal*, Phys. Solid State, 46, 1891 (2004); https://doi.org/10.1134/1.1809426.

[30] M. Rani, P K Kamlesh, S. Kumawat, U. Rani, G. Arora, and A S Verma, *Ab-Initio Calculations of Structural, Optoelectronic, Thermoelectric, and Thermodynamic Properties of Mixed-Halide Perovskites $RbPbBr_{3-x}I_x$ (x = 0 to 3): Applicable in Renewable Energy Devices*, ECS J. Solid State Sci. Technol., 12, 083006 (2023); https://doi.org/10.1149/2162-8777/acec9c.

[31] H. Huang, A. S. Susha, S. V. Kershaw, T. F. Hung, A. L. and Rogach, *Control of emission color of high quantum yield $CH_3NH_3PbBr_3$ perovskite quantum dots by precipitation temperature*, Adv. Sci., 2(9), 1500194 (2015); https://doi.org/10.1002/advs.201500194.

[32] F. Zhang, H. Zhong, C. Chen, X.-gang Wu, X. Hu, H. Huang, J. Han, B. Zou, and Y. Dong, *Brightly luminescent and color-tunable colloidal $CH_3NH_3PbX_3$(X=Br, I, Cl) quantum dots: potential alternatives for display technology*, ACS Nano, 9(4), 4533 (2015); https://doi.org/10.1021/acsnano.5b01154.

[33] L. Protesescu, S. Yakunin, M. I. Bodnarchuk, F. Krieg, R. Caputo, C. H. Hendon, R. Xi Yang, A. Walsh, and M. V. Kovalenko, *Nanocrystals of caesium lead halide perovskites ($CsPbX_3$, X=Cl, Br, and I): novel optoelectronic materials showing bright emission with wide color gamut*, Nano Lett., 15, 3692 (2015); https://doi.org/10.1021/nl5048779.

[34] J. H. Noh, S. H. Im, J. H. Heo, T. N. Mandal, and S. Il Seok, Chemical Management for Colorful, Efficient, and Stable Inorganic−Organic Hybrid Nanostructured Solar Cells, American Chemical Society, Nano Lett., 13, 1764 (2013); https://doi.org/10.1021/nl400349b.

[35] B. Suarez, V. Gonzalez-Pedro, T. S. Ripolles, R. S. Sanchez, L. Otero, and I. Mora-Sero, *Recombination study of combined halides (Cl, Br, I) perovskite solar cells*, J. Phys. Chem. Lett., 5, 1628 (2014); https://doi.org/10.1021/jz5006797.

[36] D. M. Jang, K. Park, D. H. Kim, J. Park, F. Shojaei, H. S. Kang, J. P. Ahn, J. W. Lee, and J. K. Song, *Reversible halide exchange reaction of organometal trihalide perovskite colloidal nanocrystals for full-range band gap tuning*, Nano Letter, 15, 5191 (2015); https://doi.org/10.1021/acs.nanolett.5b01430.

[37] A. Poglitsch and D. Weber *Dynamic disorder in methylammonium tri halogen oplum bates (II) observed by millimetre wave spectroscopy*, J. Chem. Phys., 87, 6373 (1987); https://doi.org/10.1063/1.453467.

[38] E. Mosconi, A. Amat, M. K. Nazeeruddin, M. Grätzel, and F. De Angelis, *First-Principles Modeling of Mixed Halide Organometal Perovskites for Photovoltaic Applications*, The J. Phys. Chem. C, 117, 13902 (2013); https://doi.org/10.1021/jp4048659.

[39] P. Umari, E. Mosconi, and F. De Angelis, *Relativistic GW calculations on $CH_3NH_3PbI_3$ and $CH_3NH_3SnI_3$ Perovskites for Solar Cell Applications*, Sci. Reports**,** 4, 4467 (2014); https://doi.org/10.1038/srep04467.

[40] L. Gil-Escrig, A.M. Sempere, M. Sessolo, and H. J BolinkJ, *Mixed Iodide-bromide Methylammonium Lead Perovskite Based Diodes for Light-emission and Photovoltaics*, Phys. Chem. Lett**,** 6, 3743 (2015); https://doi.org/10.1021/acs.jpclett.5b01716.

[41] R. A. Jishi, O. B. Ta, and A. A. Sharif, *Modeling of Lead Halide Perovskites for Photovoltaic Applications*, J. Phys. Chem. C, 118, 28344 (2014); https://doi.org/10.1021/jp5050145.

[42] J. Feng and B. Xiao, *Crystal Structures, Optical Properties, and Effective Mass Tensors of $CH_3NH_3PbX_3$ (X = I and Br) Phases Predicted from HSE06*. J. Phys. Chem. Lett, 5, 1278 (2014); https://doi.org/10.1021/jz500480m.

[43] E. Mosconi, P. Umari, and G. De Angelis, *Electronic and optical properties of $MAPbX_3$ perovskites (X = I, Br, Cl): a unified DFT and GW theoretical analysis*, Phys. Chem. Chem. Phys, 18, 27158 (2016); https://doi.org/10.1039/C6CP03969C.

[44] M. S. Alias, I. Dursun, M. I. Saidaminov, E. M. Diallo, P. Mishra, T. K. Ng, O. M. Bakr, and B. S. Ooi, *Optical constants of $CH_3NH_3PbBr_3$ perovskite thin films measured by spectroscopic ellipsometry*, Opt. Express, 24, 16586. (2016); https://doi.org/10.1364/OE.24.016586.

[45] J. S. Park, S. Choi, Y. Yan, Y. Yang, J. M. Luther, Su-Huai Wei, P. Parilla, and K. Zhu, *Electronic Structure and Optical Properties of α-CH3NH3PbBr3 Perovskite Single Crystal*, J. Phys. Chem. Lett**,** 6, 4304 (2015); https://doi.org/10.1021/acs.jpclett.5b01699.

[46] F. Sani, S. Shafie, H. N. Lim and A. O. Musa, *Advancement on Lead-Free Organic-Inorganic Halide Perovskite Solar Cells: A Review*, Materials, 11(6)**,** 1008 (2018); https://doi.org/10.3390/ma11061008.

[47] V.M. Goldschmidt, *Die gesetze der krystallochemie*, Die Naturwissenschaften, 14, 477 (1926); https://doi.org/10.1007/bf01507527.

[48] C. J. Bartel, C. Sutton, B. R. Goldsmith, R. Ouyang, C. B. Musgrave, L. M. Ghiringhelli, M. Scheffler, *New tolerance factor to predict the stability of perovskite oxides and halides*, Science Advances, 5, eaav0693 (2019); https://doi.org/10.1126/sciadv.aav0693.

[49] M. Rini, R. Tobey, N. Dean, J. Itatani, Y. Tomioka, Y. Tokura, R. W. Schoenlein, and A. Cavalleri, *Control of the electronic phase of a manganite by mode-selective vibrational excitation*, Nature, 449, 72 (2007); https://doi.org/10.1038/nature06119.

[50] C. Li, X. Lu, W. Ding, L. Feng, Y. Gao, and Z. Guo, *Formability of ABX_3 (X = F, Cl, Br, I) halide perovskites*, Acta Crystallographica Section B: Structural Science, 64, 702 (2008); https://doi.org/10.1107/S0108768108032734.

[51] Z. Xiao, Y. Yan, *Progress in theoretical study of metal halide perovskite solar cell materials*, Advanced Energy Materials, 7, 1701136 (2017); https://doi.org/10.1002/aenm.201701136.

[52] N.-G. Park, *Perovskite solar cells: an emerging photovoltaic technology*, Materials Today, 18, 65 (2015); https://doi.org/10.1016/j.mattod.2014.07.007.

[53] Y. Zhu, J. Zhang, Z. Qu, S. Jiang, Y. Liu, Z. Wu, F. Yang, W. Hu, Z. Xu, and Y. Dai, *Accelerating stability of ABX_3 perovskites analysis with machine learning*, Ceramics International, 50, 6250 (2024); https://doi.org/10.1016/j.ceramint.2023.11.349.

[54] R.D. Shannon, *Revised effective ionic radii and systematic studies of interatomic distances in halides and chalcogenides*, Acta crystallographica section A: crystal physics, diffraction, theoretical and general crystallography, 32, 751 (1976).

[55] R. A. Jishi, *Modified Becke-Johnson exchange potential: improved modeling of lead halides for solar cell applications*, AIMS Materials Science, 3(1), 149 (2016); https://doi.org/10.3934/matersci.2016.1.149.

[56] N.G. Park, *Perovskite solar cells: an emerging photovoltaic technology*, Materials Today**,** 18(2), 65 (2015); https://doi.org/10.1016/j.mattod.2014.07.007.

[57] G. Kieslich, S. Sun, and A. K. Cheetham, *An extended Tolerance Factor approach for organic–inorganic perovskites*, Chemical Science, 6**,** 3430 (2015); https://doi.org/10.1039/C5SC00961H.

[58] G.K.H. Madsen, P. Blaha, K. Schwarz, E. Sjöstedt, L. Nordström, *Efficient linearization of the augmented plane-wave method*, Physical Review B. 64, 195134 (2001); https://doi.org/10.1103/physrevb.64.195134.

[59] K. Schwarz, P. Blaha, G. K. H. Madsen, *Electronic structure calculations of solids using the WIEN2k package for material sciences*, Computer Physics Communications, 147, 71 (2002); https://doi.org/10.1016/S0010-4655(02)00206-0.

[60] P. Blaha, Peter, K. Schwarz, F. Tran, R. Laskowski, G. K. H. Madsen, and L. D. Marks, *WIEN2k: An APW+ lo program for calculating the properties of solid*s, The Journal of chemical physics, 152, 074101 (2020); https://doi.org/10.1063/1.5143061.

[61] P. Hohenberg, and W. Kohn, *Inhomogeneous electron gas*, Physical Review B**,** 136, 864 (1964); http://dx.doi.org/10.1103/PhysRev.136.B864.

[62] P. Verma, C. Singh, P. K. Kamlesh, K. Kaur, and A. S. Verma, *Nowotny-Juza phase KBeX (X = N, P, As, Sb, and Bi) half-Heusler compounds: applicability in photovoltaics and thermoelectric generators*, J. Mol. Model., 29(1), 23 (2023); https://doi.org/10.1007/s00894-022-05433-z.

[63] Y. Toual, S. Mouchou, U. Rani, A. Azouaoui, A. Hourmatallah, R. Masrour, A. Rezzouk, K. Bouslykhane, and N. Benzakour, *Probing electronic, magnetic and thermal properties of NiMnSb Half-Heusler alloy for spintronics as an environmentally friendly energy resource: A DFT+ U and Monte Carlo study*, Mater. Today Commun, 108064 (2024).

[64] M. Bonilla, D. A. Landínez-Téllez, J. A. Rodríguez, J.A. Aguiar, and J. Roa-Rojas, *Study of half-metallic behavior in Sr_2CoWO_6 perovskite by ab initio DFT calculations*, Journal of Magnetism and Magnetic Materials, 320, e397 (2018); https://doi.org/10.1016/j.jmmm.2008.02.179.

[65] F. Tran, R. Laskowski, P. Blaha, K. Schwarz, *Performance on molecules, surfaces, and solids of the Wu-Cohen GGA exchange-correlation energy functional*, Physical Review B, 75, 115131 (2007); https://doi.org/10.1103/PhysRevB.75.115131.

[66] J. P. Perdew, S. Burke and M. Ernzerhof, *Generalized gradient approximation made simple*, Physical Review Letters, 77, 3865 (1996); https://doi.org/10.1103/PhysRevLett.77.3865.

[67] A. D. Becke, and E. R. Johnson, *A simple effective potential for exchange*. The Journal of Chemical Physics, 124, 221101 (2006); https://doi.org/10.1063/1.2213970.

[68] A. D. Becke, M. R. Roussel, *Exchange Holes in Inhomogeneous Systems: A Coordinate-Space Model*. Phys. Rev. A, 39, 3761 (1989); https://doi.org/10.1103/PhysRevA.39.3761.

[69] F. Tran, P. Blaha, K. Schwarz, *Band gap calculations with Becke–Johnson exchange potential*. Journal of Physics: Condensed Matter, 19, 196208 (2007); https://doi.org/10.1088/0953-8984/19/19/196208.

[70] F. Tran, P. Blaha, *Accurate Band Gaps of Semiconductors and Insulators with a Semilocal Exchange-Correlation Potential*. Phys. Rev. Lett., 102, 226401 (2009); https://doi.org/10.1103/PhysRevLett.102.226401.

[71] D. Koller, F. Tran, P. Blaha, *Merits and Limits of the Modified Becke-Johnson Exchange Potential*. Phys. Rev. B, 83, 195134 (2011); https://doi.org/10.1103/PhysRevB.83.195134.

[72] S. Kumari, P. K. Kamlesh, L. Kumari, S. Kumar, S. Kumari, R. Singh, R. Gupta, M. S. Chauhan, and A. S. Verma, *Progress in theoretical study of lead-free halide double perovskite Na_2AgSbX_6 (X = F, Cl, Br & I) thermoelectric materials*, J. Mol. Model., 29, 195 (2023); https://doi.org/10.1007/s00894-023-05599-0.

[73] U. Rani, P. K. Kamlesh, T. K. Joshi, S. Sharma, R. Gupta, S. Al-Qaisi, and A. S. Verma, *Alkaline earth based antiperovskite $AsPX_3$ (X = Mg, Ca, and Sr) materials for energy conversion efficient and thermoelectric applications*., Physica Scripta, 98(7), 075902 (2023); https://doi.org/10.1088/1402-4896/acd88a.

[74] P. K. Kamlesh, R. Agarwal, U. Rani, and A. S. Verma, *First-principles calculations of inherent properties of Rb based state-of-the-art half-Heusler compounds: Promising materials for renewable energy applications*, Phys. Scr., 96(11), 115802 (2021); https://doi.org/10.1088/1402-4896/ac119d.

[75] H. J. Monkhorst, J. D. Pack, *Special points for Brillouin-zone integrations*, Physical Review B, 13, 5188 (1976); https://doi.org/10.1103/physrevb.13.5188.

[76] D. Weber, *$CH_3NH_3PbX_3$, ein Pb(II)-System mit kubischer Perowskitstruktur / $CH_3NH_3PbX_3$, a Pb(II)-System with Cubic Perovskite Structure*. Zeitschrift Für Naturforschung B, 33(12), 1443 (1978); https://doi.org/10.1515/znb-1978-1214.

[77] S. Ryu, J. H. Noh, N. J. Jeon, Y. C. Kim, W. S. Yang, J. Seo, and S. I. Seok, *Voltage output of efficient perovskite solar cells with high open-circuit voltage and fill factor*. Energy Environ. Sci., 7, 2614 (2014); https://doi.org/10.1039/C4EE00762J.

[78] N. Kitazawa, Y. Watanabe, and Y. Nakamura, *Optical properties of $CH_3NH_3PbX_3$ (X= halogen) and their mixed-halide crystals*. Journal of materials science, 37, 3585 (2002); https://doi.org/10.1023/A:1016584519829.

[79] L. Bokdam, M., Sander, T., Stroppa, A., Picozzi, S., Sarma, D. D., Franchini, C., & Kresse, G. Role of Polar Phonons in the Photo Excited State of Metal Halide Perovskites. Scientific Reports, 6, (2016); https://doi.org/10.1038/srep28618.

[80] M. Roknuzzaman, M.A. Hadi, M.A. Ali, M.M. Hossain, N. Jahan, M.M. Uddin, J.A. Alarco, K. Ostrikov, *First hafnium-based MAX phase in the 312 family, Hf_3AlC_2: A first-principles study*, Journal of Alloys and Compounds, 727, 616 (2017); https://doi.org/10.1016/j.jallcom.2017.08.151.

[81] T. Zhao, W. Shi, J. Xi, D. Wang, and Z. Shuai, *Intrinsic and extrinsic charge transport in CH3NH3PbI3 perovskites predicted from first-principles*, Scientific Reports, 6, 19968 (2016); https://doi.org/10.1038/srep19968.

[82] J. K. Bairwa, M. Rani, P K Kamlesh, R. Singh, U. Rani, S. Al-Qaisi, T. Kumar, S. Kumari, and A S Verma, *Modelling and simulation of multifaceted properties of X_2NaIO_6 (X = Ca and Sr) double perovskite oxides for advanced technological applications*, J Mol Model., 19, 379(2023); https://doi.org/10.1007/s00894-023-05786-z.

[83] Pallavi, C. Singh, P. K. Kamlesh, R. Gupta, and A. S. Verma, *Thermoelectric performance of cadmium based LiCdX (X = N, P, As, Sb & Bi) filled-tetrahedral semiconductors: Applications in green energy resources*, *Pramana*, J. Phys., 97(4), 162 (2023); https://doi.org/10.1007/s12043-023-02627-9.

А. Міна[1], Дж.К. Баірва[1], С. Кумарі[1], У. Рані[2], П.К. Камлеш[4], А.П. Сінгх[1], А.С. Верма[3,5]

Структурні, електронні та оптоелектронні характеристики гібридного перовскіту $CH_3NH_3PbBr_3$ на основі розрахунків з перших принципів

[1]Кафедра фізики, Університет Раджастхана, Джайпур, Раджастан, Індія;
[2]Кафедра фізики, Інститут інженерії та технології Нойди, Велика Нойда, Індія;
[3]Відділ досліджень та інновацій, Школа прикладних і природничих наук, Університет Уттаранчал, Дехрадун, Уттаракханд, Індія;
[4]Школа фундаментальних і прикладних наук, Нірванський університет Джайпур, Джайпур, Раджастан, Індія;
[5]Університетський центр досліджень і розвитку, факультет фізики, Університет Чандігарха, Мохалі, Пенджаб, Індія,
ajay_phy@rediffmail.com

Використовуючи код Wien2k, проведено обчислення з перших принципів у рамках методу повного потенціалу лінеаризованої розширеної плоскої хвилі (FP-LAPW) і теорії функціоналу густини (DFT) для визначення сталих гратки, міжатомних відстаней, щільності станів і зонної структури. Для оцінки структурних та електронних властивостей було використано три різні обмінно-кореляційні потенціали: PBE, наближення локальної щільності (LDA) і узагальнене градієнтне наближення Wo-Cohen (WC-GGA). Виявлено, що розраховані постійні ґратки чудово узгоджуються з експериментальними даними, підтверджуючи точність обчислювального підходу. Для підтвердження структурної стабільності матеріалу розраховано коефіцієнт толерантності Голдсміта та фактор октаедричності. Пряма заборонена зона 2,32 еВ, яка спостерігається в точці R-R, свідчить про сприятливі умови для застосувань у сонячні енергетиці. Подальше покращення забороненої зони було досягнуто за допомогою методу mBJ. Були проаналізовані оптичні властивості, включаючи діелектричну функцію, показник заломлення, коефіцієнт екстинкції, коефіцієнт поглинання, коефіцієнт відбивання, функцію втрат енергії електронів і фотопровідність. Примітно, що дослідження вказує на надійність $CH_3NH_3PbBr_3$, як поглинаючого шару в сонячних елементах, що підтверджується розширеною забороненою зоною та іншими оптичними властивостями.

Ключові слова: WIEN2k, DFT, Перовскіти на основі металевого свинцю (MLHP), сонічна батарея, оптоелектроніка.